

# Synthesis and Reactions of 3d Metal Complexes with the Bulky Alkoxide Ligand [OC<sup>t</sup>Bu<sub>2</sub>Ph]

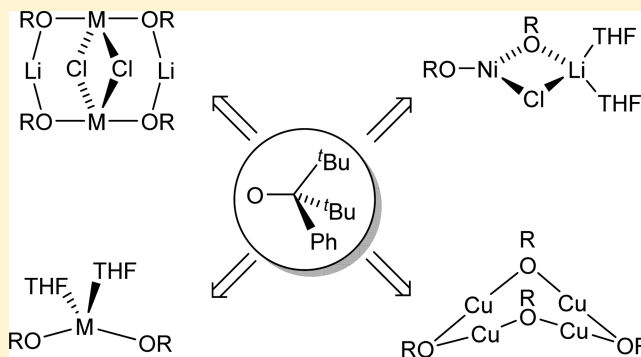
James A. Bellow,<sup>†,¶</sup> Maryam Yousif,<sup>†,¶</sup> Dong Fang,<sup>†,‡</sup> Eric G. Kratz,<sup>†</sup> G. Andrés Cisneros,<sup>\*,†</sup> and Stanislav Groysman<sup>\*,†</sup>

<sup>†</sup>Department of Chemistry, Wayne State University, Detroit, Michigan 48202, United States

<sup>‡</sup>Department of Chemistry, University of Wisconsin-Madison, Madison, Wisconsin 53706, United States

## Supporting Information

**ABSTRACT:** Treatment of NiCl<sub>2</sub>(dme) and NiBr<sub>2</sub>(dme) (dme = dimethoxyethane) with 2 equiv of LiOR (OR = OC<sup>t</sup>Bu<sub>2</sub>Ph) forms the distorted trigonal planar complexes [NiLiX(OR)<sub>2</sub>(THF)<sub>2</sub>] (THF = tetrahydrofuran) **5** (X = Cl) and **6** (X = Br). The reaction of CuX<sub>2</sub> (X = Cl, Br) with 2 equiv of LiOR affords the Cu(I) product Cu<sub>4</sub>(OR)<sub>4</sub> (**7**). The same product can be obtained using the Cu(I) starting material CuCl. NMR studies indicated that the reduction of Cu(II) to Cu(I) is accompanied by the oxidation of the alkoxide RO<sup>-</sup> to form the alkoxy radical RO<sup>•</sup>, which subsequently forms *tert*-butyl phenyl ketone by  $\beta$ -scission. Treatment of compounds **1–4** ([M<sub>2</sub>Li<sub>2</sub>Cl<sub>2</sub>(OR)<sub>4</sub>], M = Cr–Co) with thallium hexafluorophosphate allowed the isolation of the distorted tetrahedral complexes of the form M(OR)<sub>2</sub>(THF)<sub>2</sub> for M = Mn (**8**), Fe (**9**), and Co (**10**). Cyclic voltammetry performed on compounds **8–10** demonstrated irreversible oxidations for all complexes, with the iron complex **9** being the most reducing. Complex **9** shows a reactivity toward PhIO and Ph<sub>3</sub>SbS to form the corresponding dinuclear iron(III) complexes Fe<sub>2</sub>(O)(OR)<sub>4</sub>(THF)<sub>2</sub> (**11**) and Fe<sub>2</sub>(S)(OR)<sub>4</sub>(THF)<sub>2</sub> (**12**), respectively. X-ray structural studies were performed, showing that the Fe–O–Fe angle for complex **11** is 176.4(1)° and that the Fe–S–Fe angle for complex **12** is 164.83(3)°.



## INTRODUCTION

Alkoxides and related phenoxides and siloxides are commonly used as ancillary ligands in coordination chemistry and catalysis.<sup>1–4</sup> However, the majority of alkoxide complexes involve early transition metals, as alkoxides are  $\pi$ -donors and bind stronger to the more electron-deficient metals.<sup>5</sup> Well-defined mid- and late-transition metal complexes of alkoxides are relatively rare due to the destabilizing interaction of the filled d orbitals on the metal with the p orbitals on the alkoxides.<sup>1</sup> The ensuing basicity of the alkoxide lone pairs leads to the formation of polymetallic clusters via bridging.<sup>1</sup> The proclivity of alkoxides to form clusters can be overcome by two different approaches: (1) making the alkoxide sterically hindering,<sup>6–9</sup> or (2) decreasing the nucleophilicity of the alkoxide lone pairs.<sup>10</sup> Demonstrating the first approach, Power and co-workers reported middle and late transition metal complexes stabilized by alkoxides featuring three large groups at the central carbon (OCR<sub>3</sub>, R = <sup>t</sup>Bu, Cy, Ph).<sup>8</sup> Pursuing the second approach, Doerrer and co-workers have recently described late transition metal complexes ligated by perfluorinated alkoxides.<sup>10</sup> They have demonstrated that fluorination diminishes  $\pi$ -basicity, prevents bridging, and leads to the formation of stable monomeric low-coordinate late (Ni, Cu) metal centers. They also demonstrated that fluorinated

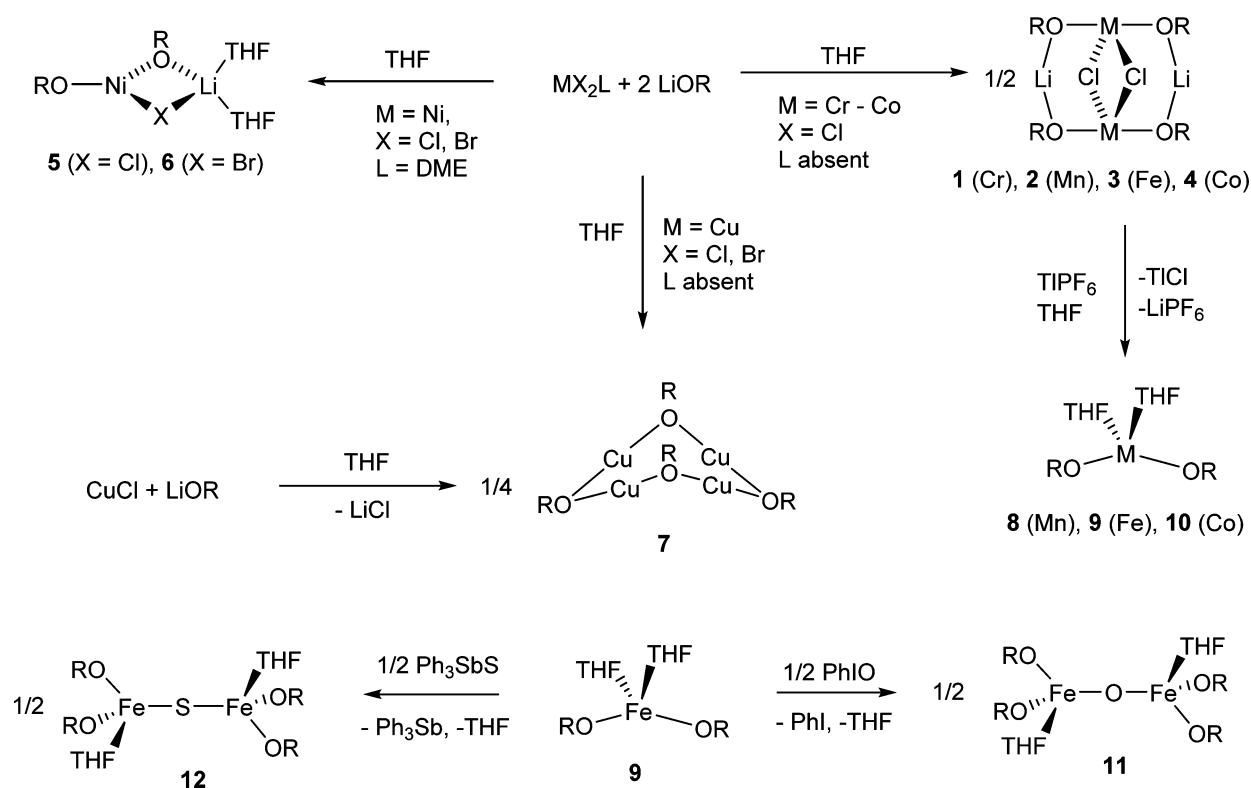
alkoxides (and related aryloxides) are capable of supporting Cu(III) complexes.

We seek low-coordinate mononuclear complexes that, upon reaction with an organic azide, will form reactive nitrene functionality. We surmised that alkoxide ligation at a middle-to-late 3d metal would lead to highly reactive metal–nitrene as (i) alkoxides are weak  $\sigma$ -donors, which should render metal–nitrene electron-deficient and (ii) at the same time, alkoxides are capable of  $\pi$ -donation, which is expected to interfere with  $\pi$ -bonding from the nitrene functionality. As we are interested in  $\pi$ -basic alkoxides, we decided to pursue a nonfluorinated bulky alkoxide ligand. Our ligand of choice was [OC<sup>t</sup>Bu<sub>2</sub>Ph].<sup>11</sup> The steric bulk of [OC<sup>t</sup>Bu<sub>2</sub>Ph] is comparable to the bulkiest alkoxide, [OC<sup>t</sup>Bu<sub>3</sub>], previously utilized by Wolczanski and co-workers<sup>7</sup> and Power and co-workers.<sup>8</sup> By replacing one of the <sup>t</sup>Bu groups by a Ph group we hoped to improve its packing and crystallinity. Furthermore, the phenyl group is tunable, allowing the ability to add additional steric bulk if needed. In our previous publications, we reported that [OC<sup>t</sup>Bu<sub>2</sub>Ph] (OR thereafter) reacts with MCl<sub>2</sub> precursors (M = Cr, Mn, Fe, and Co) to form novel alkoxide clusters of [M<sub>2</sub>Li<sub>2</sub>Cl<sub>2</sub>(OR)<sub>4</sub>] composition featuring rare seesaw geometry at transition metal

Received: December 11, 2014

Published: June 4, 2015

Scheme 1. Synthesis of the Alkoxide Complexes 1–12 Reported in This Paper



centers (1–4, Scheme 1 below).<sup>11a</sup> For Fe, we have also demonstrated that  $[\text{Fe}_2\text{Li}_2\text{Cl}_2(\text{OR})_4]$  can be transformed into a mononuclear complex  $\text{Fe}(\text{OR})_2(\text{THF})_2$  (THF = tetrahydrofuran), which displays intriguing reactivity with an alkyl (adamantyl, Ad) azide, enabling its one-electron reductive coupling to form the metal-ligated hexazene species  $[\text{AdNNNNNNAd}]^{2-}$ .<sup>11b</sup> Following these initial results, we became interested in the synthesis of other middle-to-late transition metal bis(alkoxide) complexes, specifically, those of Cr, Mn, Co, and Ni. Furthermore, the intriguing reactivity of the  $\text{Fe}(\text{OR})_2(\text{THF})_2$  complex with azides prompted us to investigate the reactivity of  $\text{Fe}(\text{OR})_2(\text{THF})_2$  and other alkoxide complexes in our study in related atom- and group-transfer reactions. Herein we report the coordination chemistry of  $[\text{OC}^t\text{Bu}_2\text{Ph}]$  with 3d metals ( $\text{M} = \text{Cr} - \text{Cu}$ ) and the reactions of the resulting metal complexes with [O]- and [S]-atom transfer reagents.

## RESULTS AND DISCUSSION

**Reactivity of  $\text{MX}_2$  ( $\text{M} = \text{Cr} - \text{Ni}$ ) with LiOR: Formation of Seesaw Clusters  $[\text{M}_2\text{Li}_2\text{Cl}_2(\text{OR})_4]$  Versus Heterodinuclear  $[\text{MLiX}(\text{OR})_2(\text{THF})_2]$  Complexes.** Scheme 1 describes the formation of various  $[\text{M}(\text{OR})_2]$  complexes obtained in this study. Four distinctly different structural types were observed: (i)  $[\text{M}_2\text{Li}_2\text{Cl}_2(\text{OR})_4]$  clusters in which the seesaw transition metal centers are ligated by two [OR] and two Cl ligands,<sup>11a</sup> (ii) heterodinuclear  $[\text{MLiX}(\text{OR})_2(\text{THF})_2]$  complexes displaying trigonal transition metal centers with two [OR] and one X ligands, (iii) mononuclear  $[\text{M}(\text{OR})_2(\text{THF})_2]$  complexes, and (iv) tetranuclear  $\text{Cu}_4(\text{OR})_4$  complex.

As previously described, treatment of  $\text{CrCl}_2$ ,  $\text{MnCl}_2$ ,  $\text{FeCl}_2$ , and  $\text{CoCl}_2$  with 2 equiv of LiOR in THF, followed by recrystallization from hexanes, affords  $[\text{M}_2\text{Li}_2\text{Cl}_2(\text{OR})_4]$  clusters.<sup>11a</sup> The reactions were postulated to proceed through

the three-coordinate intermediate  $[\text{MLiCl}(\text{OR})_2(\text{THF})_2]$ , which was directly observed only for Fe.<sup>11a</sup> In contrast, the reaction of  $\text{NiCl}_2(\text{dme})$  ( $\text{dme} = \text{dimethoxyethane}$ ) with 2 equiv of LiOR followed by recrystallization from hexanes forms stable orange  $[\text{NiCl}(\text{OR})_2\text{Li}(\text{THF})_2]$  (5, 65% yield). Similarly, the reaction of  $\text{NiBr}_2(\text{dme})$  with 2 equiv of LiOR forms red-orange  $[\text{NiBr}(\text{OR})_2\text{Li}(\text{THF})_2]$  (6, 63% yield). Complexes 5 and 6 demonstrate solution magnetic moments of  $3.0 \pm 0.2$  and  $3.1 \pm 0.2 \mu_B$ , respectively, indicating two unpaired electrons (expected spin-only moment is  $2.8 \mu_B$ ). The structure of 6 is given in Figure 1, and the structure of isomorphous 5 is given in

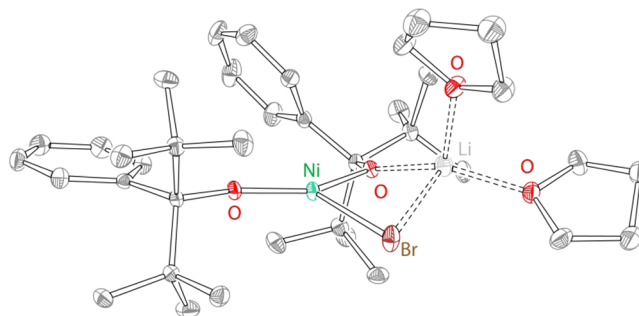


**Figure 1.** Structure of  $[\text{NiLiBr}(\text{OR})_2(\text{THF})_2]$  (6), 50% ellipsoids. H atoms were omitted for clarity. Dashed lines indicate largely ionic interactions with lithium.

the Supporting Information. Both compounds display distorted trigonal planar geometry at the Ni centers (sum of angles at Ni  $360.0^\circ$ ). Selected structural data for 5 and 6 are presented in Table 1. For comparison, we included the structural data for one of the seesaw clusters (3).

Table 1. Selected Structural Data for the Compounds Reported in This Paper

complex	M–OR <sub>terminal</sub> (Å)	M–OR <sub>bridging</sub> (Å)	OR–M–OR (deg)	THF–M–THF (deg)	M–X–M (deg)	M = X (or M–X–M) (Å)
3		1.91(1) <sup>a</sup>	174.0(2)			
5	1.748(1)	1.871(1)	147.67(6) <sup>c</sup>			
6	1.747(1)	1.872(1)	148.24(5) <sup>c</sup>			
7		1.85(1) <sup>d</sup>	165(4) <sup>b</sup>			
8	1.899(1)		130.0(1)	86		
9	1.838(1)		138.7(1)	83		
10	1.8491(1)		131.1(1)	88		
11	1.82(1)		108.6(1)		176.4(1)	1.8031(3)
12	1.80(1) <sup>b</sup>		117(4) <sup>a</sup>		164.83(3)	2.186(4) <sup>a</sup>

<sup>a</sup>Average of two bonds/angles. <sup>b</sup>Average of four bonds/angles. <sup>c</sup>The angle between terminal and bridging alkoxides. <sup>d</sup>Average of eight bonds.

**Reactivity of Cu(II) and Cu(I) Precursors with LiOR: Formation of Cu<sub>4</sub>(OR)<sub>4</sub> Tetramer.** We also investigated the reactivity of copper(II) precursors with LiOR. Treatment of an orange solution of CuBr<sub>2</sub> in THF with 2 equiv of LiOR in ether forms immediately a dark red solution. The red color, however, instantaneously changes to amber, light blue, and eventually to colorless. Solvent removal, followed by recrystallization of the product from hexanes at –35 °C, leads to the formation of the colorless Cu(I) cluster [Cu<sub>4</sub>(OR)<sub>4</sub>] (7) isolated in 42% yield. The reaction of CuCl<sub>2</sub> with LiOR under identical conditions forms the same product in 46% yield. [Cu<sub>4</sub>(OR)<sub>4</sub>] (7) can be also obtained from a copper(I) precursor, CuCl, in 51% yield.

We characterized compound 7 by <sup>1</sup>H and <sup>13</sup>C NMR spectroscopy, X-ray crystallography, and elemental analysis. The <sup>1</sup>H NMR spectrum of 7 contains one kind of OR resonance, consistent with the approximate D<sub>2d</sub> symmetry of the structure. The X-ray structure of compound 7 is given in Figure 2. Compound 7 is a tetramer of [CuOR] units featuring

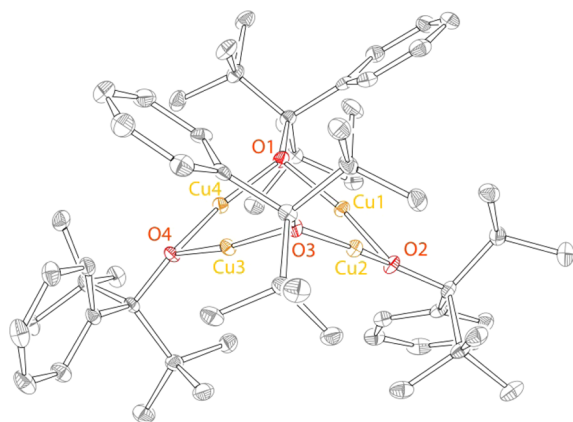


Figure 2. Structure of [Cu<sub>4</sub>(OR)<sub>4</sub>] (7), 50% ellipsoids. H atoms and THF solvent were omitted for clarity.

nearly linear Cu(I) centers each ligated by two alkoxides. Four Cu(I) centers form a plane with Cu...Cu distances ranging from 2.64 to 2.72 Å. The alkoxides coordinate below and above the Cu<sub>4</sub> plane, leading to the overall “butterfly” structure. Such geometry can be also described in terms of two Cu<sub>2</sub>(OR)<sub>3</sub> planes (O4Cu4Cu3O1O3 and O2Cu1Cu2O1O3) intersecting at 115° angle. Several related compounds exist in the literature, namely, Cu<sub>4</sub>(O<sup>t</sup>Bu)<sub>4</sub>, Cu<sub>4</sub>(OAr)<sub>4</sub> (Ar = C<sub>6</sub>H<sub>3</sub>Ph<sub>2</sub>), and Cu<sub>4</sub>(OCPh<sub>3</sub>)<sub>4</sub>.<sup>1,12</sup> Of the above, Cu<sub>4</sub>(O<sup>t</sup>Bu)<sub>4</sub> and Cu<sub>4</sub>(OAr)<sub>4</sub> are planar, while Cu<sub>4</sub>(OCPh<sub>3</sub>)<sub>4</sub> has a similar (to compound 7) butterfly molecular geometry, with a wider angle (141°) between the Cu<sub>2</sub>(OR)<sub>3</sub> planes.

Most remarkably, all of the previous Cu<sub>4</sub>(OR)<sub>4</sub> compounds were obtained from copper(I) precursors, while in our case it is also obtained from various copper(II) starting materials. It is possible that at the first step, an analogous (to [NiLiBr(OR)<sub>2</sub>(THF)<sub>2</sub>] or [FeLiCl(OR)<sub>2</sub>(THF)<sub>2</sub>]) product [CuLiX(OR)<sub>2</sub>(THF)<sub>2</sub>] is formed (see below for its calculated structure). We also note that calculations (see below) indicate that its dimerization to form [Cu<sub>2</sub>Li<sub>2</sub>X<sub>2</sub>(OR)<sub>4</sub>] is unlikely. The copper center in [CuLiX(OR)<sub>2</sub>(THF)<sub>2</sub>] then undergoes reduction, and the alkoxide constitutes the only possible reducing agent in such transformation. Upon oxidation, it is expected to form an [RO] radical. The cyclic voltammetry (CV) of LiOR demonstrates an irreversible oxidation at the relatively accessible potential of 0.51 V versus FeCp<sub>2</sub>/FeCp<sub>2</sub><sup>+</sup> (Figure 3). We note that tertiary alkoxide is not commonly

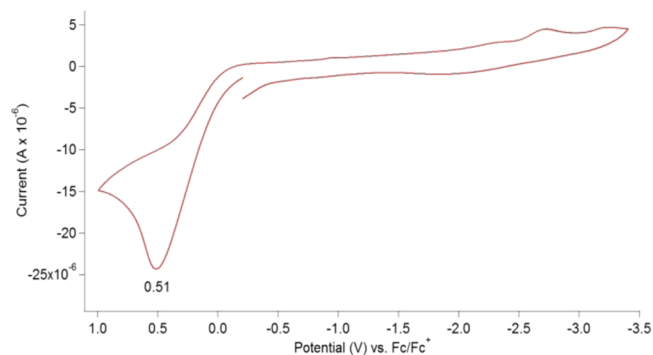
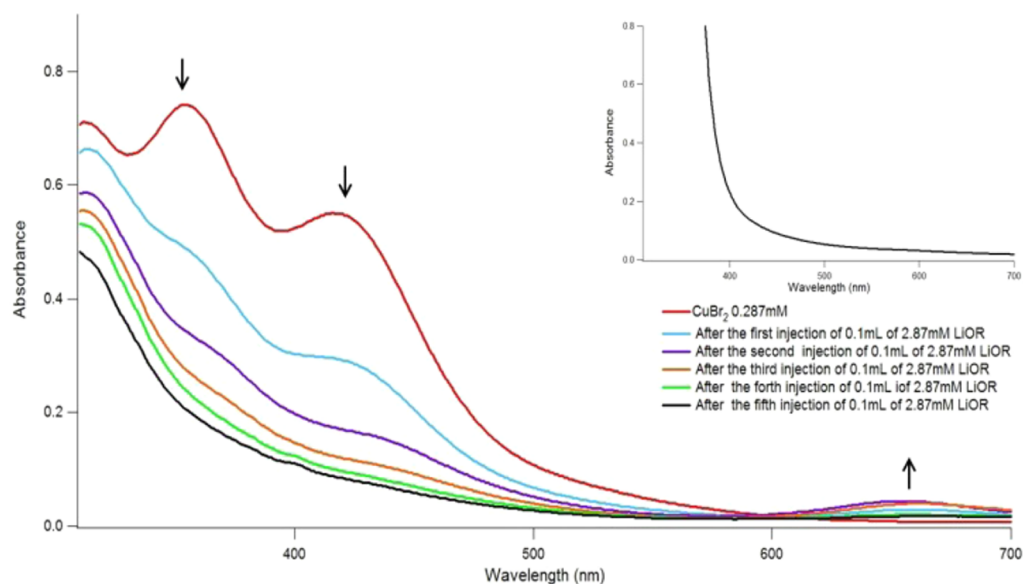


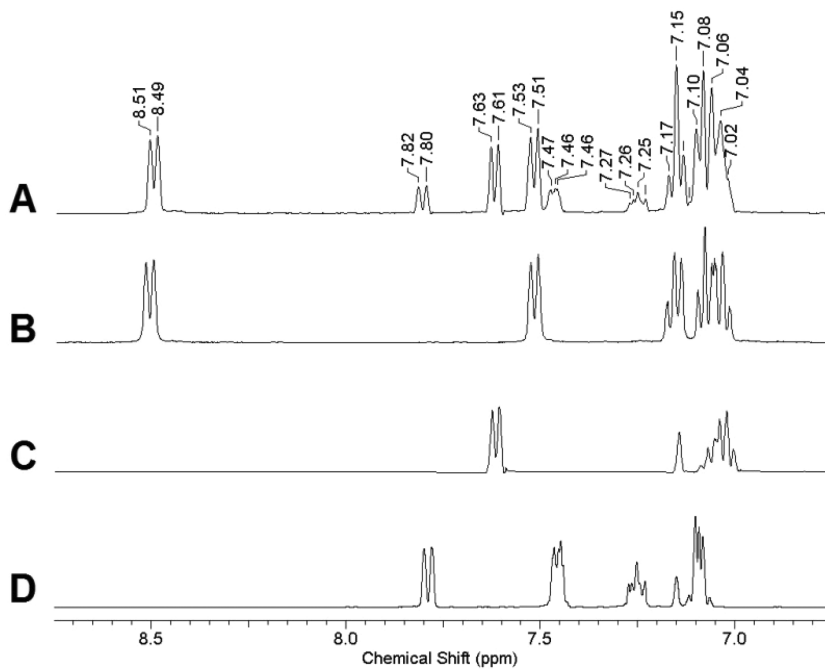
Figure 3. CV of LiOR in THF, (0.1 M [NBu<sub>4</sub>](PF<sub>6</sub>), 25 °C, platinum working electrode, 100 mV/s scan rate).

observed as a reductant.<sup>1</sup> Furthermore, we are unaware of any previous examples in which Cu(II) is reduced by an alkoxide. We also note that the inability of [OR] to support even Cu(II) centers stands in sharp contrast to the behavior of fluorinated alkoxides capable of supporting Cu(III).<sup>10</sup>

We followed the reaction of CuBr<sub>2</sub> with 2 equiv of LiOR by UV–vis spectroscopy and NMR spectroscopy. The addition of 0.5 mL of a 2.86 M LiOR solution into an orange 0.286 mM solution of CuBr<sub>2</sub> (2.5 mL in THF) immediately leads to a color change to colorless. A UV–vis scan performed ca. 10 s after the addition revealed the final product (Supporting Information, Figure S22). We tried to perform the reaction at 0 or at –78 °C. Still, the reaction was too fast at 0 °C, and no reaction took place at –78 °C. However, batch-wise addition of the solution of LiOR to the solution of CuBr<sub>2</sub> (Figure 4) at room temperature (RT) provided clear evidence for the existence of an intermediate. The red trace in Figure 4



**Figure 4.** UV–vis spectra following the batch-wise addition of LiOR to the solution of  $\text{CuBr}_2$ . (inset) The spectrum of the  $\text{Cu}_4(\text{OR})_4$ .

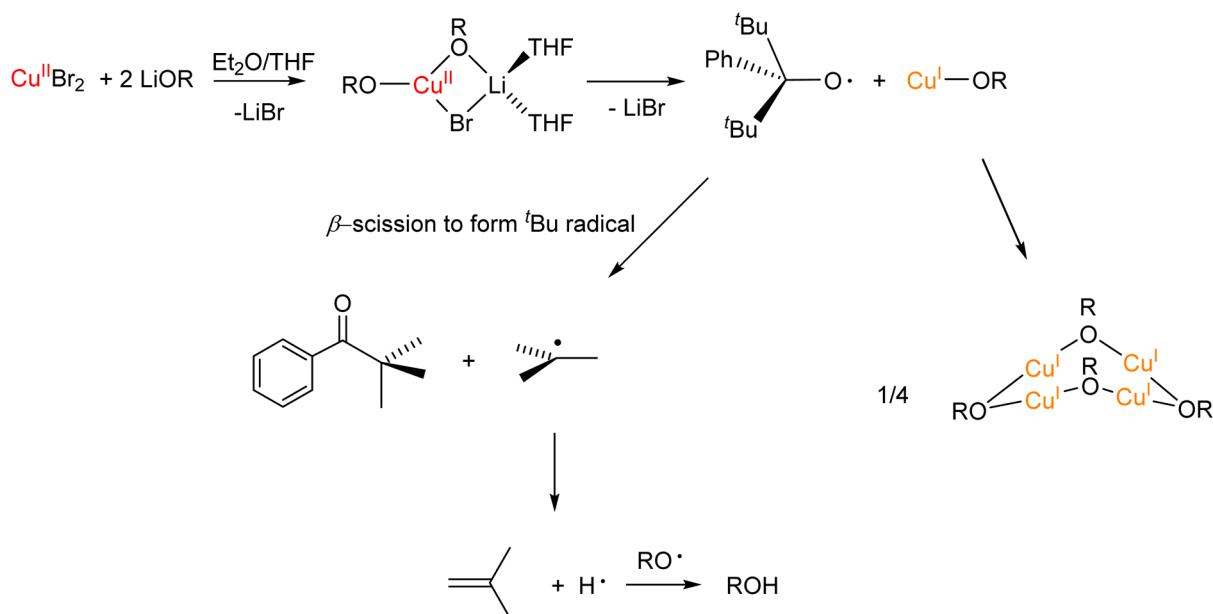


**Figure 5.** (A)  $^1\text{H}$  NMR spectrum of an aliquot of the crude reaction mixture displayed at 6.8 to 8.8 ppm. (B)  $^1\text{H}$  NMR spectrum of  $\text{Cu}_4(\text{OR})_4$  in the same region. (C)  $^1\text{H}$  NMR spectrum of *tert*-butyl phenyl ketone (2,2-dimethyl-1-phenylpropan-1-one). (D)  $^1\text{H}$  NMR spectrum of HOR.

represents the UV–vis spectrum of the 0.287 mM solution of  $\text{CuBr}_2$  in THF (2.5 mL) that is dominated by two signals at 415 and 355 nm. The addition of 0.1 mL of a 2.87 mM solution of LiOR (0.4 equiv) leads to the decline in the intensity of the absorption peaks attributed to  $\text{CuBr}_2$  and an appearance of a new signal at 660 nm. The spectrum of the final product of the reaction ( $\text{Cu}_4(\text{OR})_4$ , see the black spectrum in the inset of Figure 4) is nearly featureless. Thus, the peak at 660 nm belongs to the short-lived intermediate of the reaction. The addition of another batch of LiOR (purple trace, next 0.4 equiv) causes further increase in the intensity of the signal at 660 nm, which is accompanied by a decrease in the intensity of the signals at 415 and 355 nm. The next addition (orange trace) leads to a further decrease in the spectrum of the starting

material, while the signal attributed to the intermediate persists. Further additions of the alkoxide (green and black traces, 2 equiv total of LiOR) lead to the disappearance of the 660 nm signal.

To gain further insight into the reaction mechanism, we also analyzed the reaction by means of  $^1\text{H}$  NMR spectroscopy. UV–vis spectroscopy indicates that the reaction is complete within several minutes. The reaction of  $\text{CuBr}_2$  with 2 equiv of LiOR in tetrahydrofuran in the presence of internal standard trimethoxybenzene was allowed to stir at RT for 30 min, after which an aliquot was taken, and its  $^1\text{H}$  NMR spectrum was collected in  $\text{C}_6\text{D}_6$ . Figure 5A demonstrates the aromatic region of the spectrum; the full spectrum is given in Figure S6 in the Supporting Information. For comparison, Figure 5 also

Scheme 2. Proposed Pathway to the Formation of  $[\text{Cu}_4(\text{OR})_4]$ , *tert*-Butyl Phenyl Ketone, and HOR

demonstrates NMR spectra of clean  $\text{Cu}_4(\text{OR})_4$  (**B**), *tert*-butyl phenyl ketone (**C**), and HOR (**D**) presented in the same region. Full spectra are given in the Supporting Information. Spectrum **A** demonstrates that the crude reaction mixture contains  $\text{Cu}_4(\text{OR})_4$ . In addition, resonances attributed to *tert*-butyl phenyl ketone and HOR are observed as well. Using the internal standard (trimethoxybenzene), we quantified the overall amount of the “[OR]” or the OR derivatives detected (quantification was done based on the *tert*-butyl resonance). We observe formation of 0.012 mmol of  $\text{Cu}_4(\text{OR})_4$  (0.048 mmol of “Cu(OR)”), 0.026 mmol of *tert*-butyl phenyl ketone, and 0.022 mmol of HOR. Given the amount of LiOR used (0.156 mmol), we account for ~62% of [OR]; it is consistent with observed yield of  $\text{Cu}_4(\text{OR})_4$  (60%). Furthermore, these data also suggest that for each equivalent of Cu(OR), we are forming ~0.5 equiv of *tert*-butyl phenyl ketone and HOR each.

Combined with the UV–vis data presented in Figure 4, the detection and quantification of various reaction products provides a key to the understanding of the reaction mechanism (Scheme 2). We propose that  $[\text{CuLiBr}(\text{OR})_2(\text{THF})_2]$  forms first, as observed or proposed for Cr–Ni. Next, the Cu–OR bond undergoes a homolytic bond cleavage to form “ $\text{Cu}^{\text{I}}(\text{OR})$ ”, which tetramerizes to form  $\text{Cu}_4(\text{OR})_4$ . The remaining alkoxy radical undergoes  $\beta$ -scission, which has been previously observed for alkoxy radicals.<sup>13</sup> The  $\beta$ -scission produces *tert*-butyl phenyl ketone and *tert*-butyl radical, which may decompose to give isobutylene and hydrogen atom that couples with the alkoxy radical to give HOR. The formation of HOR is also possible via the H atom abstraction by the alkoxy radical from the solvent.<sup>13</sup> We did not observe isobutylene: the reaction takes place in THF/ether mixture, and the solvent/volatiles needed to be removed prior to dissolving the reaction mixture in  $\text{C}_6\text{D}_6$ .

**Synthesis and Characterization of Mononuclear Bis-(alkoxide) complexes  $\text{M}(\text{OR})_2(\text{THF})_2$ .** At the next step, we turned to the synthesis of neutral mononuclear species lacking complexed LiX. We postulated that complexed halide anions can be abstracted by the addition of  $\text{Tl}^+$ , which is expected to form insoluble  $\text{TlX}$ . Treatment of  $[\text{M}_2\text{Li}_2\text{X}_2(\text{OR})_4]$  (**2–4**)

complexes with  $\text{TlPF}_6$  in THF affords colorless  $\text{Mn}(\text{OR})_2(\text{THF})_2$  (**8**, 60%), colorless  $\text{Fe}(\text{OR})_2(\text{THF})_2$  (**9**),<sup>11b</sup> and violet  $\text{Co}(\text{OR})_2(\text{THF})_2$  (**10**, 49%). We note that compounds **8–10** are related to the previously described  $\text{M}(\text{OR}')_2(\text{THF})_2$  ( $\text{OR}' = \text{OCPh}_3$ ,  $\text{M} = \text{Mn, Fe, Co}$ )<sup>8e,f</sup> and the more recently synthesized  $\text{Mn}(\text{OAr})_2(\text{THF})_2$  complexes.<sup>14</sup> Surprisingly, no reaction with  $\text{TlPF}_6$  was observed for the heterodinuclear Ni complexes **5** and **6**. Workup of the reaction mixture in both cases led to the reisolation of the starting materials. Treatment of the Cr-containing seesaw cluster **1** with  $\text{TlPF}_6$  failed to produce the corresponding  $\text{Cr}(\text{OR})_2(\text{THF})_2$  species.

Compounds **8–10** were characterized by IR spectroscopy, <sup>1</sup>H NMR spectroscopy, solution magnetic measurements, UV–vis spectroscopy, CV, and X-ray crystallography. Compounds **8–10** demonstrate  $\mu_{\text{eff}}$  values of  $5.5 \pm 0.3 \mu_{\text{B}}$  for Mn (**8**),  $4.7 \pm 0.3 \mu_{\text{B}}$  for Fe (**9**), and  $3.6 \pm 0.3 \mu_{\text{B}}$  for Co (**10**) at RT (measured by Evans method using average of three measurements). The corresponding calculated spin-only values for the high-spin Mn(II), Fe(II), and Co(II) centers are 5.9, 4.9, and  $3.9 \mu_{\text{B}}$ , respectively. Thus, the observed magnetic moments of distorted tetrahedral complexes are close to spin-only magnetic moments. We note that two-coordinate bis(aryloxy) Fe and Co complexes demonstrate significantly higher  $\mu_{\text{eff}}$  values due to a considerable orbital contribution.<sup>15,16</sup> The IR spectra of **8–10** are given in Supporting Information, Figure S12. As anticipated, compounds **8–10** give rise to almost identical IR spectra with prominent C–O stretches around  $1100 \text{ cm}^{-1}$ . UV–vis spectra are given in the Supporting Information. Colorless **8** and **9** are nearly featureless in the observed region. Pale violet **10** ( $\text{Co}(\text{OR})_2(\text{THF})_2$ ) gives rise to several weak transitions in the visible region. The most significant peak at 734 nm exhibits an extinction coefficient of  $175 \text{ M}^{-1} \text{ cm}^{-1}$ .

CVs of compounds **8–10** are given in Figure 6. CVs were obtained in THF, using  $[\text{NBu}_4](\text{PF}_6)$  as the electrolyte, and are reported versus ferrocene/ferrocenium couple. Only irreversible oxidations are observed, peaking at 0.45 V for  $\text{Fe}(\text{OR})_2(\text{THF})_2$  (onset at ~0 V), 1.27 V for  $\text{Co}(\text{OR})_2(\text{THF})_2$  (onset at ~0.5 V), and 1.43 V for  $\text{Mn}(\text{OR})_2(\text{THF})_2$  (onset at

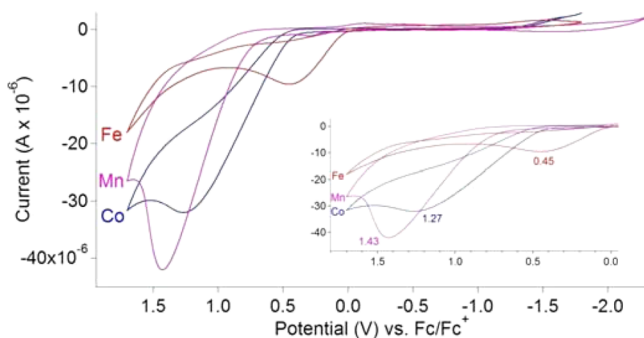


**Figure 6.** CVs of compounds **8–10** in THF, (0.1 M  $[\text{NBu}_4](\text{PF}_6)$ , 25 °C, platinum working electrode, 100 mV/s scan rate).

$\sim 0.7$  V), respectively. The lack of reversible features in the CVs is not uncommon in the electrochemistry of complexes supported by bulky monodentate alkoxides,<sup>9c,10a,17</sup> indicating that the complexes undergo rearrangement upon oxidation. No reductions were observed up to  $-2$  V. This electrochemical behavior demonstrates that (i) the complexes in the present form are unlikely to reach lower than M(II) oxidation states and that (ii) while the oxidation of Fe(II) is relatively accessible, it may be less feasible for the Mn and Co compounds **8** and **10**.

X-ray quality crystals of compounds **8–10** were obtained from hexanes at  $-35$  °C. The structure of **9** has been previously reported,<sup>11b</sup> and the structures of compounds **8** and **10** are presented in Figures 7 and 8. Selected structural data for **8–10**

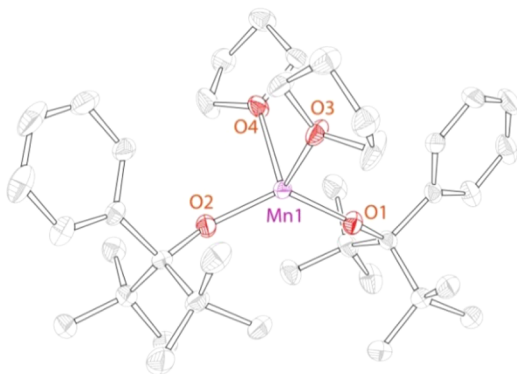


**Figure 7.** Structure of  $\text{Mn}(\text{OR})_2(\text{THF})_2$  (**7**), 50% probability ellipsoids. H atoms are omitted for clarity.

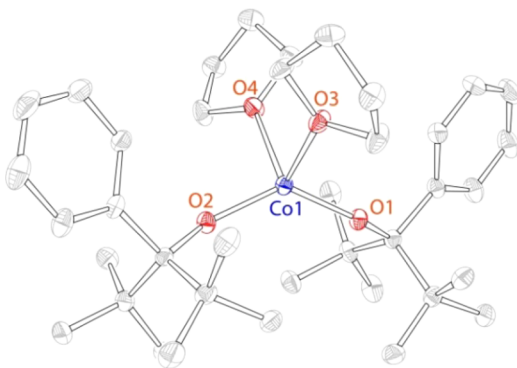


**Figure 8.** Structure of  $\text{Co}(\text{OR})_2(\text{THF})_2$  (**9**), 50% probability ellipsoids. H atoms are omitted for clarity.

are summarized in Table 1. Similarly to the previously described **9**, compounds **8** and **10** are distorted tetrahedral complexes featuring wide RO–M–OR angles ( $130^\circ$  for **8**,  $131^\circ$  for **10**), and narrow THF–M–THF angles ( $86^\circ$  for **8**,  $88^\circ$  for **10**). Related distorted tetrahedral  $\text{Mn}(\text{OAr})_2(\text{THF})_2$  and  $\text{Fe}(\text{OCPh}_3)_2(\text{THF})_2$  were previously reported, both exhibiting RO–M–OR angles of  $140^\circ$ .<sup>14,8f</sup>

**Atom-Transfer Chemistry of Complexes 8–10.** The electrochemical studies indicate that  $\text{Fe}(\text{OR})_2(\text{THF})_2$  (**9**) is more reducing than  $\text{Mn}(\text{OR})_2(\text{THF})_2$  and  $\text{Co}(\text{OR})_2(\text{THF})_2$  complexes **8** and **10**. The reactivity of **8–10** in group-transfer chemistry correlates with these observations. We have previously demonstrated that **9** reductively couples adamantyl azide to form Fe(III)-bound hexazene.<sup>11b</sup> In contrast, no reaction with adamantyl azide was observed for the Mn and Co complexes **8** and **10**. Similarly, **9** undergoes a reaction with an oxo-transfer reagent (PhIO) and a sulfur-atom transfer reagent ( $\text{Ph}_3\text{SbS}$ )<sup>18</sup> to furnish  $\text{Fe}_2(\text{O})(\text{OR})_4(\text{THF})_2$  (**11**) and  $\text{Fe}_2(\text{S})(\text{OR})_4(\text{THF})_2$  (**12**), respectively (Scheme 1). Treatment of **8** and **10** with the oxo- and sulfur atom-transfer reagents under similar reaction conditions failed to produce the oxidized products.

The structures of **11** and **12** are given in Figure 9. Both complexes feature distorted tetrahedral Fe(III) centers ligated by two terminal alkoxides, one THF ligand, and a bridging oxo (**11**) or sulfido (**12**) ligand. Thus, similarly to the previously reported hexazene complex  $[\text{Fe}_2^{\text{III}}(\text{AdNNNNNAd})(\text{OR})_4]$ ,<sup>11b</sup> the Fe centers retain the bis(alkoxide) ligation upon chemical transformation. Complex **11** displays crystallographic  $C_2$  symmetry, with only half the molecule occupying the asymmetric unit. The Fe–O–Fe angle is  $176.4(1)^\circ$ , and the Fe–( $\mu_2$ -O) distance is  $1.8031(3)$  Å. The Fe–S–Fe angle in the non- $C_2$ -symmetric **12** is  $164.8^\circ$ , and the Fe–S bond distances are  $2.1821(5)$  and  $2.1901(5)$  Å. While  $\text{Fe}_2(\mu_2\text{-O})$  compounds are common in the literature, compound **12** is one of the few known di-Fe(III) complexes in which the Fe centers are bridged by a single sulfide.<sup>19</sup> The IR spectra of compounds **11** and **12** in the  $600\text{--}1700$   $\text{cm}^{-1}$  region are presented in Figure 10 below. The overlay of the spectra demonstrates a significant structural similarity, with the exception of the strong peak at  $795$   $\text{cm}^{-1}$  that is observed only for compound **11** and is therefore assigned to the Fe–oxo stretch. The Fe–sulfido stretch is expected to occur in the far-IR region ( $<500$   $\text{cm}^{-1}$ ) and was not observed. The UV–vis spectra of **11** and **12** are given in Supporting Information, Figures S20 and S21. The spectrum of pale yellow-orange **11** exhibits a weak absorption (shoulder) around 500 nm. Unlike other compounds reported in this paper, sulfur-containing deep red **12** demonstrates relatively intense absorptions around 497 ( $21\,350$   $\text{M}^{-1}\text{cm}^{-1}$ ) and 339 ( $7570$   $\text{M}^{-1}\text{cm}^{-1}$ ) nm.

**Density Functional Theory Calculations of the Stability of the Seesaw “Dimers” Versus the Trigonal Planar “Monomers”.** Intrigued by the stark difference in the reactivity between Cr–Co and Ni, Cu, we performed density functional theory (DFT) calculations on the stability of selected  $[\text{MLiX}(\text{OR})_2(\text{THF})_2]$  (“monomers”) and  $[\text{M}_2\text{Li}_2\text{X}_2(\text{OR})_4]$  (“dimers”). We calculated the energy change during the formation of dimers as in Scheme 3 both in gas phase and in solvent environment. The relative change in electronic energy ( $\Delta E_0$ ) during the reaction in gas phase for Ni (39.1 kcal/mol) is indeed larger than the other metals (Co, 31.5 kcal/mol; Fe, 34.6 kcal/mol; Mn, 28.2 kcal/mol; Cr, 32.6 kcal/mol). When solvation effects are included in the calculations, the dimers

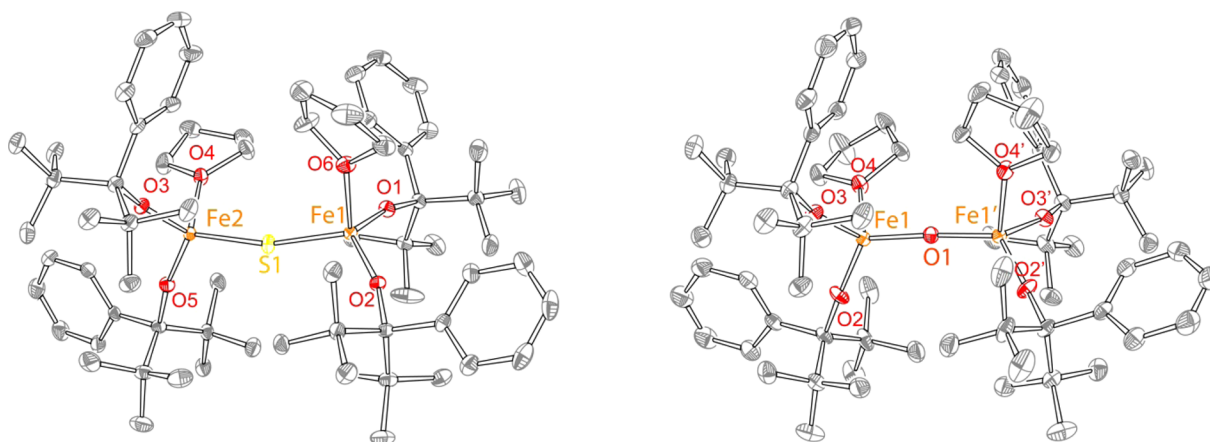


Figure 9. Structures of **11** (right) and **12** (left), 50% probability ellipsoids. H atoms are omitted for clarity.

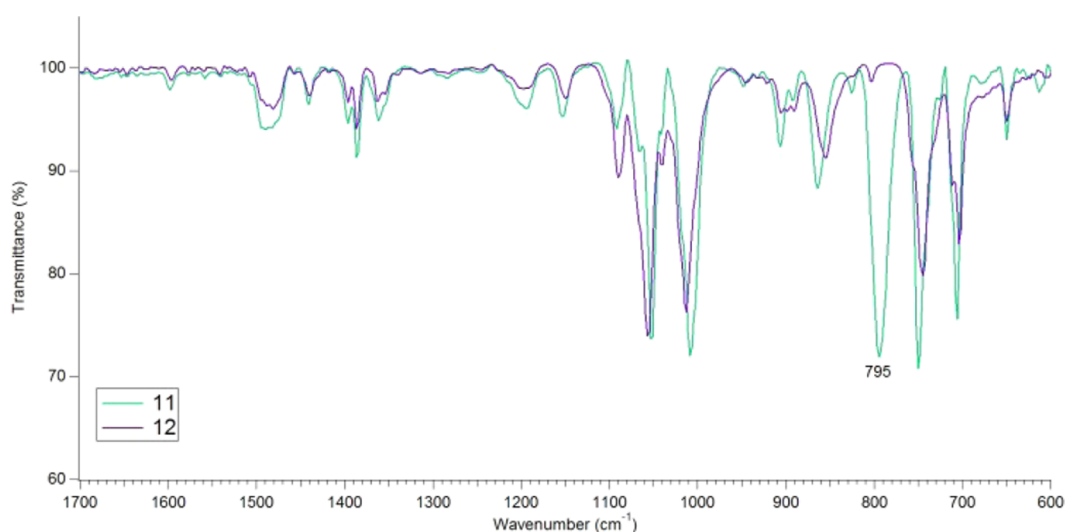
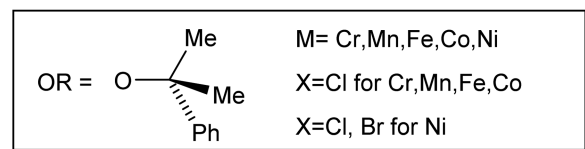
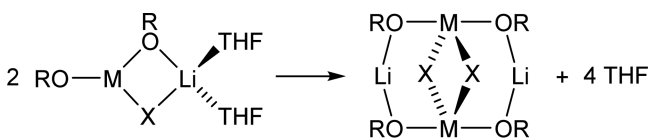


Figure 10. IR spectra of compounds **11** and **12** in the 600–1700  $\text{cm}^{-1}$  range.

### Scheme 3. A Transformation Used to Determine the Free Energy Differences between Monomers and Dimers



become more stable; however, this effect is smaller for the Ni complexes than for the other metal complexes. Most of the change in the free energy of reaction is due to the entropic term ( $-T\Delta S$ ), which corresponds to  $-27.2$  and  $-19.6$  kcal/mol for Ni and Mn, respectively, in the gas phase. In THF (hexane), the contribution for Ni is smaller in comparison,  $-26.3$  ( $-26.9$ ) kcal/mol. In contrast, the entropic contribution decreases to  $-29.5$  ( $-29.0$ ) kcal/mol for Mn in THF (hexane). As a result, a relatively large electronic energy change and small stabilization from the solvation effects lead to a positive  $\Delta G$  for Ni (6.9

kcal/mol in hexane, 10.5 kcal/mol in THF) compared to Mn ( $-5.2$  kcal/mol in hexane,  $-6.0$  kcal/mol in THF).

To try to rationalize the observed Cu chemistry, we performed computational analysis on the hypothetical Cu monomer and dimer. The optimized structure of the Cu monomer is given in Supporting Information, Figure S25, and the calculated structure of the dimer is given in Figure 11. The structure of the Cu monomer is similar to the structures of the Ni and Fe monomers, whereas the optimized structure of the Cu dimer is strikingly different. In the case of the dimer formation with Cu, the  $\Delta G$  for the gas phase reaction was calculated to be 5.7 kcal/mol, which is similar to that found for the Co complex. When the calculations were repeated in THF (hexane), the free energy of reaction decreases to  $-1.7$  (2.9) kcal/mol. While the calculations suggest that the dimer is stable in THF, note that the Br atoms are not bridging between the Cu atoms in the optimized geometry (Figure 11). Furthermore, repeating the calculations at the B97D/SDDall level of theory did not predict a stable product. The relative free energy change due to solvation effects ( $\Delta\Delta G$ )<sup>23</sup> was found to be  $-7.3$  and  $-2.8$  kcal/mol in THF and hexane, respectively. This is comparable to the values for the Mn complex, which are  $-9.6$  and  $-8.8$  kcal/mol in THF and hexane, respectively. This suggests that the overall reaction is stabilized by THF to a similar extent for the Mn and Cu complexes (in contrast with

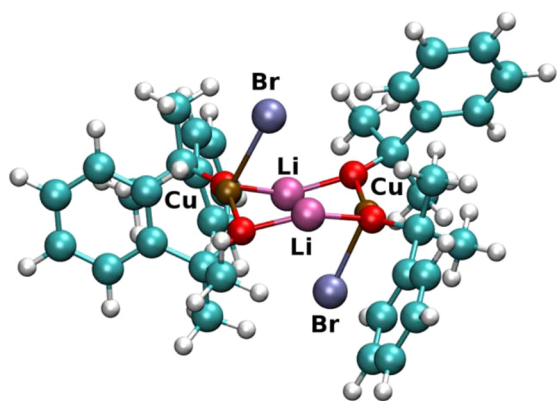


**Figure 11.** Calculated structures of the for the Cu dimer. The isovalue is 0.5, and data are plotted in the range of  $-0.07 < \text{sign}(\lambda^2)\rho < 0.07$  au.

the Ni complex). However, the  $\Delta G$  for the reaction with Cu is less favorable by 4.6 kcal/mol than for the Mn complexes. While the approximations employed in the calculations may introduce errors in the  $\Delta G$  values,<sup>24</sup> clearly the Cu dimer is significantly less stable than those containing Cr–Co. We also performed NBO<sup>25</sup> and NCI<sup>26–30</sup> analysis on the Cu dimer (see Supporting Information for details) that suggests that most of the interactions between the two halves of the dimer are primarily weak van der Waals interactions.

## SUMMARY AND CONCLUSIONS

We have described coordination chemistry of a bulky alkoxide ligand [O<sup>t</sup>Bu<sub>2</sub>Ph] with 3d transition metals Cr–Cu. The ligand demonstrates versatile behavior at the 3d metal centers, forming mononuclear  $M(\text{OR})_2(\text{THF})_2$ ,  $M = \text{Mn, Fe, Co}$  and heterodinuclear  $(M_2\text{Li}_2\text{Cl}_2(\text{OR})_4)$  and  $\text{MLiCl}(\text{OR})_2(\text{THF})_2$  complexes. DFT calculations demonstrate that the formation of seesaw complexes  $M_2\text{Li}_2\text{Cl}_2(\text{OR})_4$  is preferred for  $M = \text{Cr–Co}$ , whereas for Ni the  $\text{MLiX}(\text{OR})_2(\text{THF})_2$  species are more stable. Surprisingly,  $\text{Cu}^{\text{II}}(\text{OR})_2$ -type complexes are not stable, decomposing to give  $[\text{Cu}^{\text{I}}(\text{OR})]_4$  and the organic products consistent with the transient alkoxy radical. All complexes under investigation demonstrate coordination of two alkoxides to a single transition metal center. Electrochemical and reactivity studies indicate that hard alkoxide ligation prohibits redox chemistry at the mononuclear Mn and Co centers in  $M(\text{OR})_2(\text{THF})_2$ . The corresponding Fe(II) complex  $\text{Fe}(\text{OR})_2(\text{THF})_2$ , however, demonstrates rich group-transfer and atom-transfer chemistry, enabling formation of Fe(III)-hexazene,<sup>11b</sup> Fe(III)-( $\mu_2$ -oxo), and Fe(III)-( $\mu_2$ -sulfido) species. We are currently investigating the reactivity of the Fe complex  $\text{Fe}(\text{OR})_2(\text{THF})_2$  in other redox transformations.

## EXPERIMENTAL SECTION

**General Methods and Procedures.** All reactions involving air-sensitive materials were executed in a nitrogen-filled glovebox. Compounds 1–4 and 9, as well as the lithium salt of the ligand (LiOR), were synthesized according to previously reported procedures.<sup>11</sup> Thallium hexafluorophosphate, copper(II) chloride, copper(II) bromide, and copper(I) chloride were purchased from Strem. Manganese(II) chloride, cobalt(II) chloride, nickel(II) chloride dimethoxyethane, nickel(II) bromide dimethoxyethane, and triphenylstibine sulfide were purchased from Aldrich. Iodosobenzene was purchased from TCI. All materials were used as received. All solvents were purchased from Fisher Scientific and were of HPLC grade. The

solvents were purified using an MBRAUN solvent purification system and stored over 3 Å molecular sieves. Compounds 5–12 were characterized by <sup>1</sup>H and <sup>13</sup>C NMR spectroscopy, IR spectroscopy, UV–vis spectroscopy, solution-state magnetic susceptibility, X-ray crystallography, CV, and elemental analysis. NMR spectra were recorded at the Lumigen Instrument Center (Wayne State Univ.) on a Varian Mercury 400 MHz NMR spectrometer in C<sub>6</sub>D<sub>6</sub> or C<sub>6</sub>D<sub>5</sub>CD<sub>3</sub> at RT. Chemical shifts and coupling constants (*J*) were reported in parts per million ( $\Delta$ ) and Hertz, respectively. IR spectra were recorded on a Shimadzu IR-Affinity1 FT-IR spectrometer as paratone oil mull suspensions. UV–vis spectra were obtained in a Shimadzu UV-1800 spectrometer. Solution-state effective magnetic moments were determined using the Evans method,<sup>20</sup> and diamagnetic corrections were calculated using the Pascal's constants method;<sup>21</sup> three independent measurements were performed for each sample (see Supporting Information for further details). Electrochemical properties were determined using CV on a BAS Epsilon system in a nitrogen-filled glovebox. Samples were prepared in anhydrous THF with 0.1 M tetrabutylammonium hexafluorophosphate [NBu<sub>4</sub>][PF<sub>6</sub>] as the supporting electrolyte. Redox potentials were determined with a scan rate of 100 mV/s at 25 °C by using a platinum disc working electrode (2 mm diameter), a platinum wire counter electrode, and a nonaqueous Ag<sup>+</sup>/Ag reference electrode, and referenced to ferrocene/ferrocenium couple. Elemental analyses were performed by Midwest MicroLab LLC.

**Synthesis and Characterization of Compounds.** *NiLi(Cl)(OR)<sub>2</sub>(THF)<sub>2</sub>* (5). A 5 mL diethyl ether solution of LiOR (47.7 mg, 0.211 mmol) was added in one portion to a stirred THF solution of NiCl<sub>2</sub>(dme) (23.2 mg, 0.105 mmol). The solution color changed from light orange to deep orange. The reaction was stirred for 1 h, after which the volatiles were removed in vacuo. The resulting residue was redissolved in hexane and filtered. Recrystallization from hexane at –35 °C afforded the product as orange crystals (46.9 mg, 65%). IR (cm<sup>-1</sup>): 2972 (m), 2876 (m), 1487 (w), 1391 (w), 1360 (w), 1099 (s), 1072 (m), 1043 (w), 1022 (s), 891 (m), 745 (s), 708 (s), 677(w), 650 (w).  $\mu_{\text{eff}} = 3.0 \pm 0.2 \mu_{\text{B}}$ . <sup>1</sup>H NMR (C<sub>6</sub>D<sub>6</sub>, 400 MHz)  $\delta$  14.18, 10.55, 9.74, 7.86, 0.46, 0.02, –0.44, –0.65, –2.81.  $\lambda_{\text{max}}$  ( $\epsilon$ ): 676 (22), 547 (99) M<sup>-1</sup> cm<sup>-1</sup>. Anal. Calcd for C<sub>38</sub>H<sub>62</sub>O<sub>4</sub>ClLiNi: C, 66.7; H, 9.1. Found: C, 66.7, H, 9.0.

*NiLi(Br)(OR)<sub>2</sub>(THF)<sub>2</sub>* (6). A 5 mL diethyl ether solution of LiOR (49.1 mg, 0.217 mmol) was added in one portion to a stirred THF solution of NiBr<sub>2</sub>(dme) (33.5 mg, 0.109 mmol). The solution color changed to deep orange. The reaction was stirred for 1 h, after which the volatiles were removed in vacuo. The resulting residue was redissolved in hexane and filtered. Recrystallization from hexane at –35 °C afforded the product as orange crystals (49.8 mg, 63%). IR (cm<sup>-1</sup>): 2972 (w), 2876 (w), 1522 (w), 1489 (m), 1393 (m), 1366 (w), 1098 (w), 1072 (m), 1043 (s), 1022 (w), 991 (s), 889 (m), 745 (s), 708 (s), 675 (m).  $\mu_{\text{eff}} = 3.1 \pm 0.2 \mu_{\text{B}}$  (calcd 2.83). <sup>1</sup>H NMR (C<sub>6</sub>D<sub>6</sub>, 400 MHz)  $\delta$  13.79, 10.09, 9.75, 6.88, –1.16, –2.49, –3.28.  $\lambda_{\text{max}}$  ( $\epsilon$ ): 682 (33), 559 (91) M<sup>-1</sup> cm<sup>-1</sup>. Anal. Calcd for C<sub>38</sub>H<sub>62</sub>O<sub>4</sub>BrLiNi: C, 62.7; H, 8.6. Found: C, 61.7, H, 8.0%. Our repeated attempts to obtain better elemental analysis for compound 6 failed. However, compound 6 is obtained in an identical fashion to compound 5 as large orange crystals, and its spectroscopic and magnetic data match well that of compound 5.

*Cu<sub>4</sub>(OR)<sub>4</sub>* (7) via *CuCl<sub>2</sub>*. A 5 mL diethyl ether solution of LiOR (45.2 mg, 0.200 mmol) was added in one portion to a stirred THF solution of CuCl<sub>2</sub> (13.4 mg, 0.100 mmol). The solution color immediately changed to deep red before darkening to brown. The reaction was stirred for 1 h, after which the volatiles were removed in vacuo. The resulting residue was redissolved in hexane and filtered. Recrystallization from hexane at –35 °C afforded the product as colorless crystals (26.0 mg, 46%). <sup>1</sup>H NMR (C<sub>6</sub>D<sub>6</sub>, 400 MHz)  $\delta$  8.52 (d, *J* = 8.0, 4H), 7.53 (d, *J* = 8.0, 4H), 7.17 (t, *J* = 4.0, 4H), 7.06 (m, 8H), 1.39 (s, 72H). <sup>13</sup>C NMR (C<sub>6</sub>D<sub>6</sub>, 75 MHz)  $\delta$  149.02, 130.19, 128.50, 127.47, 126.07, 125.13, 86.32, 41.61, 31.22. IR (cm<sup>-1</sup>): 3001 (w), 2951 (w), 2905 (w), 2878 (w), 1489 (w), 1389 (m), 1362 (w), 1153 (w), 1049 (s), 995 (s), 895 (w), 745 (s), 706 (s). No discernible

features in the UV–vis spectrum. Anal. Calcd for  $C_{60}H_{92}O_4Cu_4$ : C, 63.7; H, 8.2. Found: C, 63.6, H, 8.0%.

$Cu_4(OR)_4$  (**7**) via  $CuBr_2$ . A 5 mL diethyl ether solution of LiOR (47.8 mg, 0.211 mmol) was added in one portion to a stirred THF of solution of  $CuBr_2$  (23.6 mg, 0.106 mmol). The solution color rapidly changed through red, amber, and light blue before ultimately turning colorless. The volatiles were removed in vacuo. The resulting residue was redissolved in hexane and filtered. Recrystallization from hexane at  $-35$  °C afforded the product as colorless crystals (25.2 mg, 42%).  $^1H$  NMR spectrum of the product matched that of the product obtained via  $CuCl_2$ .

$Cu_4(OR)_4$  (**7**) via  $CuCl$ . This procedure is identical to that for the reaction with copper(II) halides. LiOR (49.3 mg, 0.218 mmol) was added to  $CuCl$  (21.6 mg, 0.218 mmol) to give a colorless solution. The reaction was stirred for 1 h, after which the volatiles were removed in vacuo. The resulting residue was redissolved in hexane and filtered. Recrystallization from hexane at  $-35$  °C afforded the product as colorless crystals (31.4 mg, 51%).  $^1H$  NMR matched that of the product obtained via  $CuCl_2$ .

$Mn(OR)_2(THF)_2$  (**8**). A 5.0 mL THF solution containing 27.8 mg (0.0795 mmol) of thallium(I) hexafluorophosphate was added dropwise to a 5.0 mL THF solution containing 42.6 mg (0.0397 mmol) of the dimeric manganese bis(alkoxide) complex  $[Mn_2Li_2Cl_2(OR)_4]$  (**2**). Immediately a white precipitate formed. The reaction was stirred for 1 h, after which the volatiles were removed in vacuo. Hexanes (~2.0 mL) were added to the remaining white cake, and subsequent filtration gave a pale yellow solution. Recrystallization from hexane at  $-35$  °C afforded the product as white crystals (30.4 mg, 60%). IR ( $cm^{-1}$ ): 2988 (m), 2963 (m), 2880 (m), 1377 (w), 1356 (w), 1107 (s), 1067 (m), 1026 (m), 872 (m), 745 (s), 708 (s), 642 (w).  $\mu_{eff} = 5.5 \pm 0.3 \mu_B$  (calc. 5.9). No discernible features in the UV–vis spectrum. Anal. Calcd for  $C_{38}H_{62}O_4Mn$ : C, 71.6; H, 9.8. Found: C, 71.3, H, 9.7%.

$Co(OR)_2(THF)_2$  (**10**). A 5.0 mL THF solution containing 28.1 mg (0.0806 mmol) of thallium(I) hexafluorophosphate was added dropwise to a 5.0 mL THF solution containing 43.5 mg (0.0403 mmol) of the dimeric cobalt bis(alkoxide) complex  $[Co_2Li_2Cl_2(OR)_4]$  (**4**). Immediately a white precipitate formed, and the reaction color changed from blue to violet. The reaction was stirred for 1 h, after which the volatiles were removed in vacuo. Hexanes (~2.0 mL) were added to the remaining white cake, and subsequent filtration gave a violet solution. Recrystallization from hexane at  $-35$  °C afforded the product as violet crystalline rods (25.3 mg, 49%). IR ( $cm^{-1}$ ): 2988 (w), 2967 (w), 2895 (w), 2876 (w), 1489 (w), 1381 (w), 1360 (w), 1090 (m), 1063 (m), 1018 (s), 868 (m), 745 (s), 708 (s).  $^1H$  NMR ( $C_6D_6$ , 400 MHz)  $\delta$  42.81, 24.95, 17.09, 13.05, 9.59, 9.39, 5.34.  $\mu_{eff} = 3.6 \pm 0.3 \mu_B$  (calc. 3.87).  $\lambda_{max}(\epsilon)$ : 734 (176), 578 (64), 472 (40), 386 (98)  $M^{-1} cm^{-1}$ . Anal. Calcd for  $C_{38}H_{62}O_4Co$ : C, 71.1; H, 9.7. Found: C, 70.8, H, 9.6%.

**Reaction of  $Ni(OR)_2BrLi(THF)_2$  with  $TIPF_6$ .** The nickel complex **6** (80.7 mg, 0.11 mmol) and  $TIPF_6$  (38.7 mg, 0.11 mmol) were dissolved in separate THF solutions. The thallium hexafluorophosphate solution was added dropwise to the nickel solution, leading to the formation of a white precipitate. The reaction was stirred for 1 h, after which the volatiles were removed in vacuo, and the resulting residue was taken up in hexane. After the insoluble precipitate was removed by filtration, the solution was concentrated before crystallization at  $-35$  °C was attempted. Orange crystals were isolated, but they were confirmed to be the starting complex **6** (48.8 mg, 60% recovery).

$Fe_2(O)(OR)_4(THF)_2$  (**11**). To a stirred solution of  $Fe(OR)_2(THF)_2$  (60.2 mg, 0.0943 mmol), 5 mL solution of PhIO (13.0 mg, 0.0591 mmol) in toluene was added at once. The reaction changed color slowly from light brown to orange brown. The reaction was stirred for 4 h, after which the solvent was removed. The residual was dissolved in hexanes and filtered. Crystallization from concentrated hexanes produced orange crystals at  $-35$  °C overnight (13.0 mg, 24% yield). IR ( $cm^{-1}$ ): 2970 (m), 2878 (m), 1483 (s), 1387 (s), 1053 (m), 1009 (m), 864 (s), 795 (m), 750 (m), 706 (m).  $\lambda_{max}(\epsilon)$ : 734 (176), 578 (64), 472 (40), 386 (98)  $M^{-1} cm^{-1}$ . No discernible features in the UV–vis spectrum, except for the shoulder around 480 nm.  $\mu_{eff} = 2.8 \pm$

$0.1 \mu_B$ . Anal. Calcd for  $C_{68}H_{108}Fe_2O_7$ : C, 71.1; H, 9.5. Found: C, 71.2; H, 9.3%.

$Fe_2(S)(OR)_4(THF)_2$  (**12**). To a stirred solution of  $Fe(OR)_2(THF)_2$  (86.8 mg, 0.136 mmol) in toluene, 5 mL solution of triphenylstibine sulfide (26.7 mg, 0.0693 mmol) in toluene was added at once. The solution color immediately changed from light brown to deep red. The reaction was stirred for 4 h, after which the solvent was removed. The residual was dissolved in hexanes and filtered. Crystallization from hexanes at  $-35$  °C produced deep red X-ray quality crystals (47.3 mg, 60% yield). IR ( $cm^{-1}$ ): 2990 (s), 2879 (s), 1481(s), 1150 (m), 1013 (m), 891 (s), 745 (m), 704 (m).  $\lambda_{max}(\epsilon)$ : 339 (7570), 497 (21 350)  $M^{-1} cm^{-1}$ .  $\mu_{eff} = 2.8 \pm 0.2 \mu_B$ . Anal. Calcd for  $C_{68}H_{108}Fe_2O_6S$ : C, 70.1; H, 9.3. Found: C, 70.3; H, 9.5%.

**Computational Details.** All geometry optimizations were performed at the B3LYP/SDDall level with the Gaussian09<sup>20</sup> software package as in our previous study.<sup>11a</sup> In all cases the <sup>t</sup>Bu substituents were replaced by Me groups for calculation efficiency. As shown in our previous work,<sup>11a</sup> the structure of the metal and its coordination sphere is minimally affected by this substitution. The correction to the Gibbs free energy (*G*) was calculated using the harmonic approximation using a scaling factor of 0.9806.<sup>21</sup> Since both Ni–Cl (**5**) and Ni–Br (**6**) show identical chemistry, both structures were considered for the calculations as a consistency check. No difference was observed between the complexes with the two different halides. In the case of the Mn and Ni complexes, solvation was modeled with the self-consistent reaction field (SCRf) method using the SMD solvation approach.<sup>22</sup> Two solvents were modeled: THF ( $\epsilon = 7.4257$ ) and hexane ( $\epsilon = 1.8819$ ). All optimized structures were confirmed by frequency calculations to have no imaginary frequencies. The relative stability between dimer and monomer structures was calculated by determining the Gibbs free energy change as described in Scheme 2. The NCI surfaces were calculated by the NCIPLOT<sup>26,27</sup> program. NCI plots the reduced density gradient versus the product of the sign of the second eigenvalue ( $\lambda_2$ ) of the electron-density Hessian matrix and the electron density. The peaks at low electron density characterize the noncovalent interactions.

## ■ ASSOCIATED CONTENT

### ● Supporting Information

Evans method formula and procedure, NMR, IR, and UV–vis spectra, X-ray data in cif format, optimized Cu monomer, NCI plot for the Fe dimer complex and for the hypothetical Cu dimer, optimized geometries for all monomers and dimers, and complete ref 22. The Supporting Information is available free of charge on the ACS Publications website at DOI: 10.1021/acs.inorgchem.5b00795.

## ■ AUTHOR INFORMATION

### Corresponding Authors

\*E-mail: groysman@chem.wayne.edu. (S.G.)

\*E-mail: andres@chem.wayne.edu. (A.C.)

### Author Contributions

<sup>†</sup>These authors contributed equally to this work.

### Notes

The authors declare no competing financial interest.

## ■ ACKNOWLEDGMENTS

We acknowledge Wayne State Univ. for the start-up funding and American Chemical Society Petroleum Research Fund for the current support of this project (54178-DNI3). We gratefully acknowledge computing time from Wayne State C&IT.

## ■ REFERENCES

(1) Bradley, D. C.; Mehrotra, R.; Rothwell, I.; Singh, A. *Alkoxo and Aryloxo Derivatives of Metals*; Academic Press: San Diego, CA, 2001.

- (2) Hartwig, J. F. *Organotransition Metal Chemistry: From Bonding to Catalysis*; University Science Books: Mill Valley, CA, 2010.
- (3) (a) Chisholm, M. H. *Chemtracts: Inorg. Chem.* **1992**, *4*, 273. (b) Chisholm, M. H. *J. Organomet. Chem.* **2014**, *751*, 55–59.
- (4) (a) Axtell, J. C.; Schrock, R. R.; Müller, P.; Smith, S. J.; Hoveyda, A. H. *Organometallics* **2014**, *33*, 5342–5348. (b) Gerber, L. C. H.; Schrock, R. R.; Müller, P. *Organometallics* **2013**, *32*, 2373–2378. (c) Townsend, E. M.; Schrock, R. R.; Hoveyda, A. H. *J. Am. Chem. Soc.* **2012**, *134*, 11334–11337.
- (5) (a) Shock, L. E.; Marks, T. J. *J. Am. Chem. Soc.* **1988**, *110*, 7701–7715. (b) Uddin, J.; Morales, C. M.; Maynard, J. H.; Landis, C. R. *Organometallics* **2006**, *25*, 5566–5581. (c) Rothwell, I. P. *Acc. Chem. Res.* **1988**, *21*, 153–9. (d) Rothfuss, H.; Huffman, J. C.; Caulton, K. G. *Inorg. Chem.* **1994**, *33*, 187–191.
- (6) (a) Bochmann, M.; Wilkinson, G.; Young, G. B.; Hursthouse, M. B.; Malik, K. M. A. *J. Chem. Soc., Dalton Trans.* **1980**, 1863–1871.
- (7) (a) Wolczanski, P. T. *Polyhedron* **1995**, *14*, 3335–3362. (b) Wolczanski, P. T. *Chem. Commun.* **2009**, 740–757. (c) LaPointe, R. E.; Schaller, C. P.; Wolczanski, P. T.; Mitchell, J. F. *J. Am. Chem. Soc.* **1986**, *108*, 6382–6384. (f) Neithamer, D. R.; LaPointe, R. E.; Wheeler, R. A.; Richeson, D. S.; Van Duyne, G. D.; Wolczanski, P. T. *J. Am. Chem. Soc.* **1989**, *111*, 9056–9072.
- (8) (a) Power, P. P. *J. Organomet. Chem.* **2004**, *689*, 3904–3919. (b) Hvosllef, J.; Hope, H.; Murray, B. D.; Power, P. P. *J. Chem. Soc., Chem. Commun.* **1983**, 1438–1439. (c) Murray, B. D.; Power, P. P. *J. Am. Chem. Soc.* **1984**, *106*, 7011–7015. (d) Olmstead, M. M.; Power, P. P.; Sigel, G. *Inorg. Chem.* **1986**, *25*, 1027–1033. (e) Sigel, G. A.; Bartlett, R. A.; Decker, D.; Olmstead, M. M.; Power, P. P. *Inorg. Chem.* **1987**, *26*, 1773. (f) Bartlett, R. A.; Ellison, J. J.; Power, P. P.; Shoner, S. C. *Inorg. Chem.* **1991**, *30*, 2888–2894.
- (9) (a) Groysman, S.; Villagrán, D.; Freedman, D.; Nocera, D. G. *Inorg. Chem.* **2010**, *49*, 10759–10761. (b) Groysman, S.; Villagrán, D.; Freedman, D.; Nocera, D. G. *Chem. Commun.* **2011**, *47*, 10242–10244. (c) Chambers, M. B.; Groysman, S.; Villagrán, D.; Nocera, D. G. *Inorg. Chem.* **2013**, *52*, 3159–3169.
- (10) (a) Cantalupo, S. A.; Lum, J. S.; Buzzeo, M. C.; Moore, C.; Rheingold, A. L.; Doerrer, L. H. *Dalton Trans.* **2010**, 374–383. (b) Cantalupo, S. A.; Ferreira, H. E.; Bataineh, E.; King, A. J.; Petersen, M. V.; Wojtasiewicz, T.; DiPasquale, A. G.; Rheingold, A. L.; Doerrer, L. H. *Inorg. Chem.* **2011**, *50*, 6584–6596. (c) Petersen, M. V.; Iqbal, A. H.; Zakharov, L. N.; Rheingold, A. L.; Doerrer, L. H. *Polyhedron* **2013**, *52*, 276–283. (d) Kim, M.; Zakharov, L. N.; Rheingold, A. L.; Doerrer, L. H. *Polyhedron* **2005**, *44*, 1803–1812. (e) Zheng, B.; Miranda, M. O.; DiPasquale, A. G.; Golen, J. A.; Rheingold, A. L.; Doerrer, L. H. *Inorg. Chem.* **2009**, *48*, 4274–4276. (f) Lum, J. S.; Tahsini, L.; Golen, J. A.; Moore, C.; Rheingold, A. L.; Doerrer, L. H. *Chem.—Eur. J.* **2013**, *19*, 6374–6384. (g) Tahsini, L.; Specht, S. E.; Lum, J. S.; Nelson, J. J. M.; Long, A. F.; Golen, J. A.; Rheingold, A. L.; Doerrer, L. H. *Inorg. Chem.* **2013**, *52*, 4050–4063.
- (11) (a) Bellow, J. A.; Fang, D.; Kovacevic, N.; Martin, P. D.; Shearer, J.; Cisneros, G. A.; Groysman, S. *Chem.—Eur. J.* **2013**, *19*, 12225–12228. (b) Bellow, J. A.; Martin, P. D.; Lord, R. L.; Groysman, S. *Inorg. Chem.* **2013**, *52*, 12335–12337. (c) Bellow, J. A.; Yousif, M.; Cabelof, A. C.; Lord, R. L.; Groysman, S. *Organometallics* **2015**, DOI: 10.1021/acs.organomet.5b00231.
- (12) (a) Håkansson, M.; Lopes, C.; Jagner, S. *Inorg. Chim. Acta* **2000**, *304*, 178–183. (b) Lopes, C.; Håkansson, M.; Jagner, S. *Inorg. Chem.* **1997**, *36*, 3232–3236. (c) Greiser, T.; Weiss, E. *Chem. Ber.* **1976**, *109*, 3142–3146.
- (13) For selected studies on the  $\beta$ -scission of alkoxy radicals, see: (a) Richardson, W. H.; Yelvingtoan, B.; Andrist, H.; Ertleyr, W.; Smith, S.; Johnson, T. D. *J. Org. Chem.* **1973**, *38*, 4219–4225. (b) Buback, M.; Kling, M.; Schmatz, S. *Z. Phys. Chem.* **2005**, *219*, 1205–1222. (c) Weber, M.; Fischer, H. *J. Am. Chem. Soc.* **1999**, *121*, 7381–7388.
- (14) (a) Kondaveeti, S. K.; Vaddypally, S.; Lam, C.; Hirai, D.; Ni, N.; Cava, R. J.; Zdilla, M. J. *Inorg. Chem.* **2012**, *51*, 10095–10104. (b) Deacon, G. B.; Goh, L. Y.; Jackson, W. R.; Skelton, B. W.; Chen, W.; White, A. H. *Z. Anorg. Allg. Chem.* **2010**, *636*, 1478–1483.
- (15) (a) Ni, C.; Power, P. P. *Chem. Commun.* **2009**, 5543–5545. (b) Bryan, A. M.; Long, G. J.; Grandjean, F.; Power, P. P. *Inorg. Chem.* **2014**, *53*, 2692–2698. (c) Hatanaka, T.; Miyake, R.; Ishida, Y.; Kawaguchi, H. *J. Organomet. Chem.* **2011**, *696*, 4046–4050.
- (16) For the discussion on the magnetic properties of two-coordinate complexes, see: Power, P. P. *Chem. Rev.* **2012**, *112*, 3482–3507.
- (17) Buzzeo, M. C.; Iqbal, A. H.; Long, C. M.; Millar, D.; Patel, S.; Pellow, M. A.; Saddoughi, S. A.; Smenton, A. L.; Turner, J. F. C.; Wadhawan, J. D.; Compton, R. G.; Golen, J. A.; Rheingold, A. L.; Doerrer, L. H. *Inorg. Chem.* **2004**, *43*, 7709–7725.
- (18) (a) Majumdar, S.; Stauber, J. M.; Palluccio, T. D.; Cai, X.; Velian, A.; Rybak-Akimova, E. V.; Temprado, M.; Captain, B.; Cummins, C. C.; Hoff, C. D. *Inorg. Chem.* **2014**, *53*, 11185–11196. (b) Yang, L.; Tehranchi, J.; Tolman, W. B. *Inorg. Chem.* **2011**, *50*, 2606–2612. (c) Groysman, S.; Wang, J.-J.; Tagore, R.; Lee, S. C.; Holm, R. H. *J. Am. Chem. Soc.* **2008**, *130*, 12794–12807.
- (19) (a) Berno, P.; Floriani, C.; Chiesi-Villa, A.; Guastini, C. *J. Chem. Soc., Dalton Trans.* **1989**, 551. (b) Vela, J.; Stoian, S.; Flaschenriem, C. J.; Munck, E.; Holland, P. L. *J. Am. Chem. Soc.* **2004**, *126*, 4522. (c) Dorfman, J. R.; Girerd, J. J.; Simhon, E. D.; Stack, T. D. P.; Holm, R. H. *Inorg. Chem.* **1984**, *23*, 4407. (d) Mukherjee, R. N.; Stack, T. D. P.; Holm, R. H. *J. Am. Chem. Soc.* **1988**, *110*, 1850.
- (20) Evans, D. F. *J. Chem. Soc.* **1959**, 2003–2005.
- (21) Bain, G. A.; Berry, J. F. *J. Chem. Educ.* **2008**, *85*, 532–536.
- (22) Frisch, M. J.; et al. *Gaussian 09*, Revision D.01; Gaussian, Inc.: Wallingford, CT, 2009.
- (23) Scott, A. P.; Radom, L. *J. Phys. Chem.* **1996**, *100*, 16502–16513.
- (24) Marenich, A. V.; Cramer, C. J.; Truhlar, D. G. *J. Phys. Chem. B* **2009**, *113*, 6378–6396.
- (25) Foster, J. P.; Weinhold, F. *J. Am. Chem. Soc.* **1980**, *102*, 7211–7218.
- (26) Contreras-García, J.; Johnson, E. R.; Keinan, S.; Chaudret, R.; Piquemal, J.-P.; Beratan, D. N.; Yang, W. *J. Chem. Theory Comput.* **2011**, *7*, 625–632.
- (27) Johnson, E. R.; Keinan, S.; Mori-Sánchez, P.; Contreras-García, J.; Cohen, A. J.; Yang, W. *J. Am. Chem. Soc.* **2010**, *132*, 6498–6506.
- (28) Fang, D.; Chaudret, R.; Piquemal, J.-P.; Cisneros, G. A. *J. Chem. Theory Comput.* **2013**, *9*, 2156–2160.
- (29) Fang, D.; Cisneros, G. A. *J. Chem. Theory Comput.* **2014**, *10*, 5136–5148.
- (30) Fang, D.; Lord, R. L.; Cisneros, G. A. *J. Phys. Chem. B* **2013**, *117*, 6410–6420.